Unsupported nanometer-sized copper clusters studied by electron diffraction and molecular dynamics

D. Reinhard*
Institut de Physique Expérimentale, EPFL, 1015 Lausanne, Switzerland

B. D. Hall†
Department of Physics, Massey University, Palmerston North, New Zealand

P. Berthoud‡
Institut de Physique Expérimentale, EPFL, 1015 Lausanne, Switzerland

S. Valkealahti§
Department of Physics, University of Jyväskylä, P.O. Box 35, FIN-40351 Jyväskylä, Finland

R. Monot**
Institut de Physique Expérimentale, EPFL, 1015 Lausanne, Switzerland
(Received 25 August 1997; revised manuscript received 20 April 1998)

An electron diffraction study on unsupported nanometer-sized copper clusters has been combined with molecular-dynamics calculations to investigate size-related structural effects. The experimental conditions allow slow cluster growth, close to thermodynamic equilibrium, in an inert-gas-aggregation source. A distinct structural change is observed, which is correlated with cluster size: there is a predominance of icosahedra below 3.8 nm in diameter, and a clear separation of size distributions for icosahedra and fcc particles, which are larger. These results confirm the predictions of an earlier molecular-dynamics study. Further molecular-dynamics simulations have provided information on atomic dynamics and thermal expansion of interatomic distances and are compared with experimental data. [S0163-1829(98)07228-2]

I. INTRODUCTION

In nanometer-sized particles, or clusters, the atomic arrangement may differ from the bulk crystallographic structure. This change in structure can be understood to arise from the increasingly important surface contribution to a particle's total energy. As the surface-to-volume ratio becomes large, an energetically favorable arrangement of atoms at the surface may be able to compensate for a strained internal structure. This is the case for the icosahedra and decahedra that characterize many small-particle structures. These particles feature close-packed facets, which have minimal surface tension, and can therefore overcome the energy cost of an internal structure that deviates from the bulk crystal and therefore is under stress. Experimental observations of icosahedral and decahedral structures, so-called multiply twinned particles (MTPs), are well documented in Marks' recent review of the subject.[1] One of their striking features is the existence of fivefold axes of symmetry, which are excluded from bulk crystallography due to incompatibility with translational symmetry.

If the intrinsic, size-related effects on cluster structure are to be studied experimentally, it is important that all possible interaction with the particles' surface are minimized, or avoided altogether. In particular, the influence of support (substrate or matrix) should be eliminated. This difficulty has long been recognized and has led to the development of experiments combining the techniques of molecular beams and high-energy electron-diffraction (HEED).[2–5]

On the theoretical side, powerful computing facilities have allowed a microscopic approach to the cluster-structure problem: molecular-dynamics (MD) simulations are widely used as a tool with which to study structural size effects. MD simulations allow model atomic arrangements to be ''energetically optimized'' by allowing atoms to relax, from an initial configuration, in an appropriate self-consistent force field. Knowing the space coordinates of every atom, the model cluster's total energy can be calculated and it is possible to determine which, of a set of structure types under consideration, represents the configuration of greatest stability under equilibrium conditions. When this is done for a range of sizes, the stability crossover between alternative structures can be estimated.[6–9] Beyond static features of this kind, MD simulations can also provide insight into important dynamical processes, such as thermal vibrations or melting.[10–14]

One of the current challenges for cluster-structure research is to obtain information on structural stability, for a given element and size range, simultaneously from experiments with unsupported particles and MD simulations. To date, this has been achieved only for argon. The pioneering molecular-beam electron-diffraction experiments of Farges *et al.*, interpreted on the basis of MD-optimized structure models,[15] have shown good qualitative agreement with stability calculations[5] and have established the existence of the icosahedral structure as an intrinsically stable atomic configuration in rare-gas clusters. However, in spite of many efforts from both experimental and theoretical groups, noth-

ing comparable has been achieved so far for metallic clusters. The latter are, however, of considerable interest, owing to their potential for application in the field of heterogeneous catalysis. Thus, on the one hand, the very detailed calculations of Cleveland and Landman for the case of nickel[6] are still awaiting comparison with a suitable experiment. On the other, the diffraction studies of free silver clusters conducted in Lausanne[16,17] as yet have no specific simulations to be compared to. Valkealahti and Manninen's recent MD investigations of structural stability for copper clusters[9] have, at last, made possible a comparison of MD simulation and experimental data for a metallic element, in much the same way as was done for argon.

In the present paper, we report on a HEED study of unsupported copper clusters, in a size range approximately centered on the crossover between icosahedral and face-centered cubic (fcc) structures predicted by Valkealahti and Manninen's MD calculations. Incidentally, we show that for the interpretation of experimental diffraction data, the availability of static and dynamic simulations is in itself an important advantage to assess the influence of relaxations and thermal vibrations on the diffraction process. In Sec. II, we give a brief overview of the experimental setup and describe how modifications to the previously published form of the apparatus have made the present study possible. Sections III and IV then present and discuss the main experimental findings of this study.

We have placed a substantial amount of detail, relating to the interpretation of the experiments and MD simulations, in appendices. These are briefly described at the end of the paper and are available from AIP's Physics Auxiliary Publication Service (PAPS).[18]

II. EXPERIMENT

The experimental apparatus has been described in detail in a previous publication.[4] Small particles are produced in an inert-gas-aggregation (IGA) source, where copper is evaporated (crucible temperature, T_c) into a flow of pure helium gas (pressure, P_g), injected at room temperature. The hot vapor cools rapidly, mixing with the inert gas, and supersaturates, leading to nucleation and growth of copper clusters. These clusters are transported by the flowing helium through a small nozzle at one end of the chamber. Two consecutive stages of differential pumping remove a substantial amount of the carrier gas, which contributes an unwanted background signal to the final diffraction pattern. The remaining mixture of gas and particles enters the diffraction chamber as a well-collimated molecular beam, and is probed by high-energy electrons (100 kV).

The random orientation of clusters in the beam gives rise to a diffraction pattern with radial symmetry, similar to those obtained from powder samples. A measurement of this pattern is made by recording an intensity profile along its diameter. The typical time required to obtain a single measurement is of the order of 1 min, making it possible to collect a series of diffraction patterns over a wide range of source operating conditions, without need of recharging the source. The series of measurements presented here were all obtained in the same experimental session.

The diffraction patterns recorded are the main source of data in an experiment, however, downstream from the beam crossing, amorphous-carbon-coated electron-microscope grids can be exposed to the cluster beam. This allows supported samples to be collected and later transferred to a transmission electron microscope. Both conventional and high resolution electron microscopy (HREM) have been used to examine samples, however, the reactivity of copper with the atmosphere, and its relatively weak contrast in HREM images, make the latter technique of only marginal importance in this study.

A high-temperature evaporation source, capable of working at temperatures of about 1900 °C, has been designed for this work. It is composed of a cylindrical boron nitride crucible (≈ 2 cm^3 capacity), heated by a tungsten filament and surrounded by a triple set of coaxial tantalum radiation shields. The crucible temperature T_c is measured by a thermocouple penetrating its base, and is stabilized by closed-loop control. The temperature stability, on the time scale of a single data acquisition, is ≈ 1 °C. The walls of the nucleation chamber, which are exposed to intense thermal radiation in spite of the crucible's multiple shielding, are water cooled and stay close to room temperature during the whole experiment. The inert-gas pressure in the chamber, P_g, is controlled by altering the injected volume flow rate. This is also regulated to achieve a relative stability of the order of 1%.

Various precautions have been taken to ensure cleanliness in the nucleation chamber. Prior to the experiment, the nucleation chamber is thoroughly cleaned and outgassed for several hours with dry argon (purity: 99.9999%) flowing continuously and the empty crucible heated to ≈ 1700 °C. The source must then be opened for a short time (after cooling to room temperature) and the crucible filled with copper (purity: 99.99%). The apparatus is then pumped down to its normal base pressure, which is 2×10^{-7} Torr in the diffraction chamber and $<10^{-3}$ Torr in the source chamber (which has no direct pumping). During the initial phase of the experiment, the crucible is heated slowly, again in a strong flow of argon to remove additional outgassing residues. When $T_c \approx 1000$ °C is reached, the inert gas being injected is switched from argon to helium (purity: 99.9996%).

III. EXPERIMENTAL RESULTS

The experimental results on which this study is based are presented in this section. In Sec. III A, a series of diffraction patterns from copper clusters, together with the principal results from the analysis of these data, are presented. Detailed analysis of each diffraction pattern provides extensive information about the composition of the beam. This will not be presented in full here, although in Sec. III B the detailed results for two profiles are given to illustrate the process. The final section, III C, presents an estimate of cluster temperature, based on an observation of thermal lattice expansion.

A common feature of IGA sources is that they give rise to a broad distribution of particle sizes (see, for example, Fig. 8). It is also not uncommon for beams of small metal particles to contain more than one type of structure under given source conditions. This is certainly true of our previous observations of unsupported silver particles.[16,17] In order to conduct a satisfactory analysis of diffraction data from such

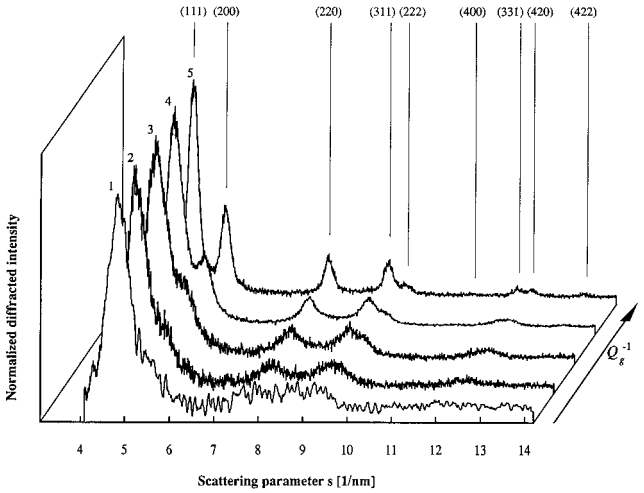

FIG. 1. Diffraction profiles obtained under the conditions described in Table I. The horizontal axis represents the scattering parameter s, where $s=2\sin\theta/\lambda$, θ is the scattering angle, and λ the electron wavelength. Scattering from carrier gas has been removed and all profiles are normalized to constant height at the principal maximum. In the case of profile 1, a simple smoothing routine has also been used to reduce statistical fluctuations. The positions and Miller indices of the fcc Bragg reflections for bulk copper at 300 K are shown above profile 5.

a sample, it is *necessary* to match the experimental data with a diffraction profile representing a combination of model particle structures. To achieve this, a large number of basis diffraction patterns are calculated and an algorithm, using the technique of simulated annealing, optimizes a combination of these to fit the data.[19] The details of this procedure are given in Appendix A.

Ideally, a range of fully relaxed structural models of clusters would be used to calculate the basis diffraction patterns for comparison with experiment. Unfortunately, the computational cost of MD simulations prevents this and we must rely on purely geometrical constructions. We have, however, investigated the consequences of doing this in Appendix B through a study of a small number of fully relaxed structures (sizes up to $\approx$10 000 atoms[20]). Relaxation in clusters causes small, but systematic, changes to occur in the corresponding diffraction profile. When fitted with profiles based on geometric forms, these changes are compensated for by artificial structural components that appear in the fitted structure size distributions. Appendix B also describes the effect of finite temperature on the diffraction patterns and the resulting choice of Debye-Waller factor.

A. Experimental diffraction results

The main experimental data used in this report are shown in Fig. 1. A series of five experimental diffraction patterns have been recorded, for which the corresponding source parameters are summarized in Table I. The profiles are presented as nearly raw data: a correction has been made to remove the contribution of background scattering due to carrier gas (which is a featureless decreasing function of scattering angle), and a simple smoothing routine has been applied to profile 1. The ordering of profiles from front to back in the figure is determined by the typical residence time for clusters in the source. Residence time is inversely proportional to Q_g, the carrier gas throughput. In Appendix C the characteristic size of clusters is shown to be correlated with Q_g^{-1}, the reciprocal of carrier gas throughput, with larger particles observed at lower throughput.

The nature of the changes in the profiles of Fig. 1 allows identification of the changing structural composition of the beam. Only profile 5 shows well-defined peaks, which can be indexed as Bragg reflections of the copper fcc lattice, indicating that this profile has a significant component of fcc particles. The remaining profiles are all dominated by MTP structures, which has the effect of broadening details in the diffraction profiles as well as giving rise to a distinct asymmetrical main peak at $s\approx 5$ nm^{-1}. We wish to stress here that this broadening is not simply size related. The diffraction profiles of MTP structures give rise to significant changes in the diffraction pattern. The distribution of intensity over the whole diffraction profile becomes important in this case, as there is no reciprocal lattice and therefore scattering is not now associated with specific diffraction angles.

Analysis of the diffraction data is performed by applying the fitting procedure described in Appendix A repeatedly to each of the experimental diffraction patterns in Fig. 1. A summary of the key results from this analysis is presented in Table II, which reports the relative abundances of each structure type, the mean diameter estimated by fitting (taking all structure types together), and, where available, the mean particle diameter as observed by transmission electron microscopy (TEM). The analysis procedure also gives information

TABLE I. The source conditions for the data in Fig. 1. T_c is the crucible temperature, P_g the helium pressure in the source, Q_g is the gas throughput, P_v the metal vapor pressure. The vapor pressures reported are deduced from the evaporation temperature using tables (Ref. 32). Note: in profile 1, the geometry of the source differs slightly, increasing the pumping speed at the first nozzle.

	Profile				
	1	2	3	4	5
T_c (K)	1974±2	1977±2	1968±2	1911±2	1916±2
P_g (mbar)	4.6±0.1	4.2±0.1	3.8±0.1	3.1±0.1	1.4±0.1
Q_g (cm^3/min)	350±2	149±2	130±2	108±2	43±2
P_v (mbar)	6.6±0.4	6.6±0.4	6.6±0.4	1.6±0.1	1.6±0.1
P_gT_c (10^2 mbar K)	91±2	83±2	75±2	59±2	27±2
Q_g^{-1} (10^{-3} min/cm^3)	2.86±0.02	6.7±0.1	7.7±0.1	9.2±0.2	23±1

TABLE II. Averaged relative abundances of each of the three structural components used to fit the experimental data. $\langle \overline{D} \rangle$ is the averaged mean diameter for the sample, obtained from the fitted distributions; $\overline{D}_{\mathrm{TEM}}$ is the mean diameter obtained by microscopy.

	Profile				
	1	2	3	4	5
fcc (%)	1±1	2±2	1±1	14±7	58±25
Icosahedra (%)	98±2	81±15	27±16	66±23	31±24
Decahedra (%)	1±1	17±17	72±16	19±19	11±11
$\langle \overline{D} \rangle$ (nm)	2.1±0.3	2.1±0.3	2.3±0.4	2.8±0.8	3.6±1.2
$\overline{D}_{\mathrm{TEM}}$ (nm)		3.1±0.2	3.4±0.1	3.6±0.1	

about the size distributions for each structure type. The values in Table II, except $\overline{D}_{\mathrm{TEM}}$, are averages over repeated fits.

From the data in Table II, a trend can be identified: starting from a dominance in fcc structure, in profile 5; and changing to a dominance in icosahedral structure, in profile 1. In Fig. 2 we report the averaged mean diameters of the fitted distributions for icosahedra and fcc particles in each of the profiles. These results are presented as a function of the reciprocal carrier gas throughput for each experiment and the bars on this figure indicate the full extent to which mean diameters were found to fluctuate when fitting was repeated. The figure gives a feel for the consistency and scatter in the results. More importantly, a trend in mean particle size can be discerned: fcc cuboctahedra are systematically larger than icosahedra. The figure uses shading to indicate the region in which the stability of each structure is expected to occur.[9]

Because the data in Fig. 2 are averaged over many fitting runs, it could be misleading to use it to make a comparison of the relative stability of the two structure types. Figure 3 shows the *difference* between mean fcc diameter and mean icosahedra diameter, averaged over fitting runs. Here, the size effect is clearly seen: the average values are all positive, indicating that there is a net tendency for fcc particles to occur at sizes greater than icosahedra when growing under the same conditions. We also found that the fitted size distributions for icosahedral and fcc particles (not shown) were well separated and had little overlap.

A similar analysis of relative sizes can be made with decahedra and fcc particles. The results in this case are inconclusive: no clear structural size effect is discernable. However, decahedra are much more difficult to distinguish from fcc particles using diffraction techniques and this makes the results of fitting more uncertain. Furthermore, decahedra are expected to appear in greatest numbers at sizes intermediate to the icosahedra and fcc regions of stability. Our observations are at least compatible with this prediction, given the appearance of decahedra in significant proportions in profiles 2, 3, and 4 with a maximum content in profile 3.

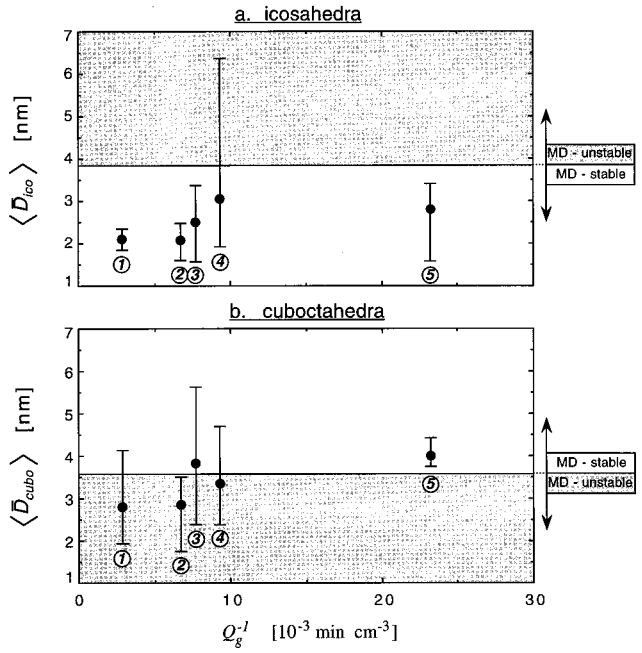

FIG. 2. Averaged mean diameters for icosahedra (a) and cuboctahedra (b) after fitting the profiles in Fig. 1. Vertical bars show the full range of mean diameters obtained by repeated fitting. The predicted regions of instability, taken from Ref. 9, are shown in gray.

B. Detailed analysis of selected diffraction data

Detailed information about the composition of the particle beam, both in terms of structural content and size distributions, is obtained as a result of fitting. To illustrate this, the results of two fitting runs are presented here.

The result of a typical fit to profile 5 is shown in Fig. 4 and Table III. Clearly, the agreement shown between fit and data in Fig. 4 is very satisfying. There is, however, a slight overestimation of diffraction intensities for $s > 7$ nm^{-1}, and also a small, but noticeable, change of horizontal scale in the fit-profile with respect to the experimental one. This is in-

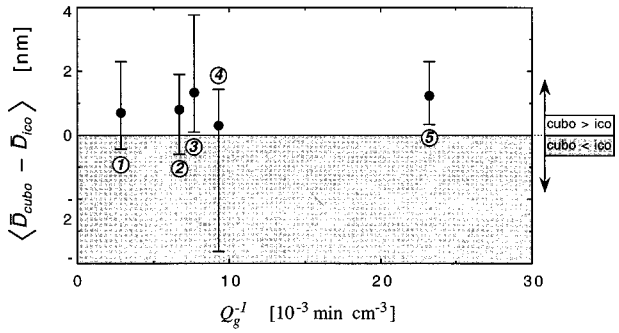

FIG. 3. The size effect is shown by the average difference in mean diameters $\langle \overline{D}_{\mathrm{cubo}} - \overline{D}_{\mathrm{ico}} \rangle$, the region where values would contradict the predicted structural size effect is shown in gray. Vertical bars show the full range of $\overline{D}_{\mathrm{cubo}} - \overline{D}_{\mathrm{ico}}$ values obtained during repeated fitting.

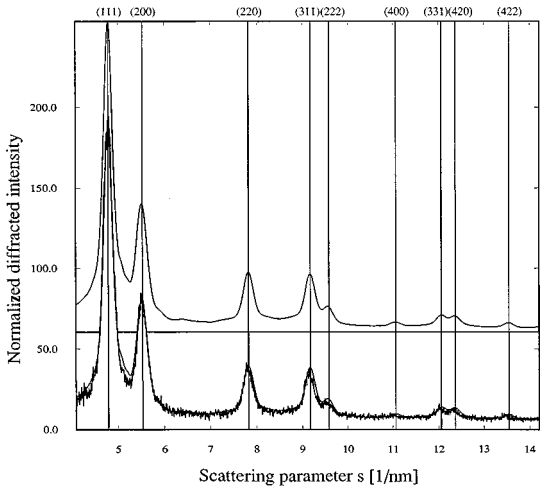

FIG. 4. Example of a typical fit to profile 5. The raw data are shown with the fit directly superimposed. The fit has also been shifted vertically, to allow inspection of distinct features. Vertical lines mark the expected positions of room-temperature crystal Bragg reflections, which are indexed at the top of the figure.

TABLE III. Size-distribution statistics for the fit to profile 5 represented in Figs. 4 and 5. The statistical parameters are introduced in Appendix A: $\overline{D}^{(i)}$ is the mean diameter; $\overline{D}_V^{(i)}$is the third moment, or the mean diameter of the volume-weighted histogram; $\eta^{(i)}$ is the relative abundance of structure i; $\gamma^{(i)}$ is the relative contribution to the total diffracted intensity.

	$\overline{D}^{(i)}$ (nm)	$\overline{D}_V^{(i)}$ (nm)	$\eta^{(i)}$ (%)	$\gamma^{(i)}$ (%)
fcc	4.2	4.4	68	56
Icosahedra	3.1	6.3	26	15
Decahedra	6.8	5.7	6	29
total (white bars)	4.0	5.1		

dicative of a slight change in lattice parameter compared to the room-temperature bulk value used in the model structures. This observation allows us to estimate cluster temperature and is discussed further in Sec. III C.

A breakdown of the structure size distributions for this fit is shown in Fig. 5. The dominant component is the fcc cuboctahedron. A small number of icosahedra are also included in the fit, some at quite large sizes, as well as a large number of small decahedra. Several of these MTP structural compo-

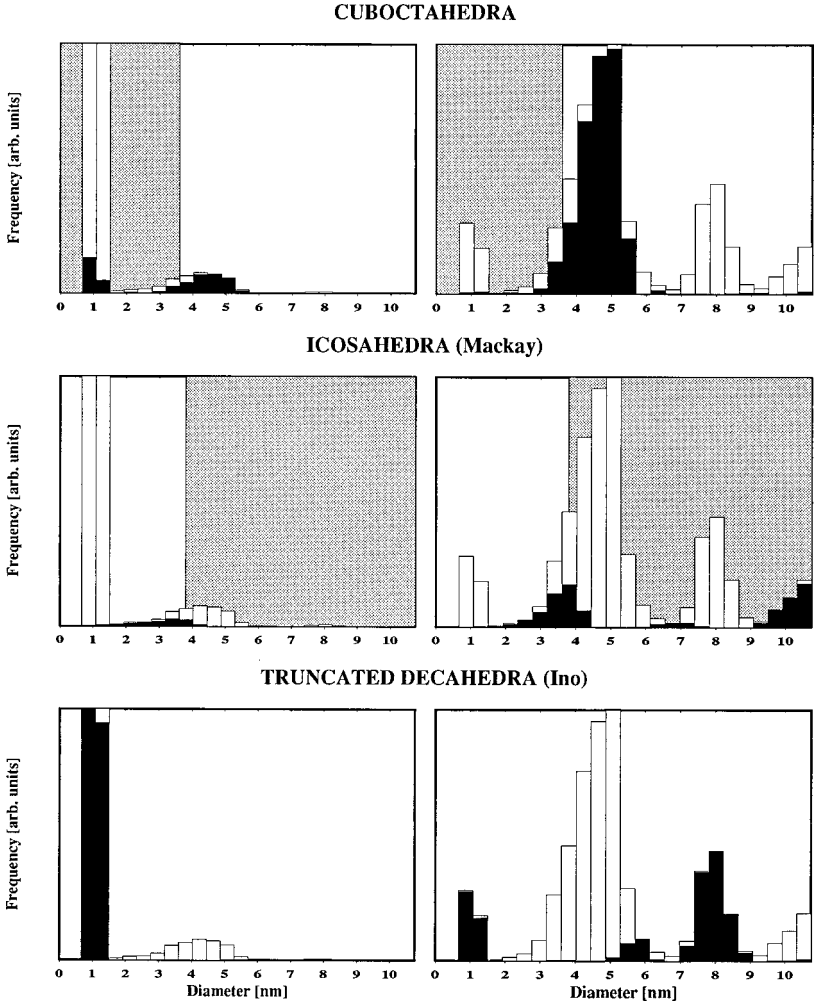

FIG. 5. Size distribution information about model structures used in the particular fit to profile 5 presented in Fig. 4. On the left, histograms of the three structure types. On the right, histograms of the volume-weighted frequency of model sizes, giving a measure of the relative contribution to the total diffracted intensity of each diameter class. The gray regions indicate regions of instability reported by Valkealahti and Manninen (Ref. 9). The white bars represent the total size distribution (i.e., all structure types together). See also statistics in Table III.

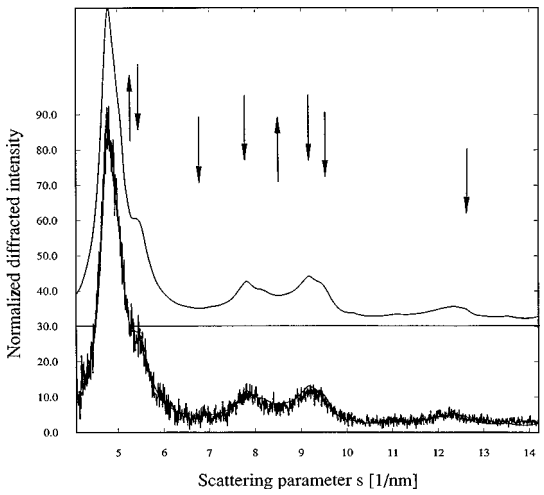

FIG. 6. Example of a typical fit to profile 2. The raw data are shown with the fit directly superimposed. The fit has also been shifted vertically, to allow inspection of distinct features. The arrows indicate in which direction the calculated profiles are altered when structures are relaxed.

nents are almost certainly artifacts. The presence of the very large icosahedra is artificial: they arise because the procedure needs to increase the relative height of the principal peak with respect to the others. This indicates that the basis profiles used in the fit do not describe the exact detail of the cluster structures in the beam: on one hand relaxation will change the relative strengths of details in the diffraction profiles (see Appendix B), on the other hand, simple twinning in fcc particles is known to enhance the strength of the (111) peak in the diffraction peak with respect to the other details recorded.[21] The small decahedra are also probably artificial. In this case, they provide broadening to the base of the (111) and (200) fcc peaks. This broadening arises in the experimental data because of imperfections in structure within particles.

Discounting these two artifacts, the results show a small icosahedral component, between 2 and 4.5 nm, some larger decahedra, and a dominance of cuboctahedra. The size range for the icosahedral and fcc components is compatible with those suggested by Valkealahti and Manninen.[9]

The result of a typical fit to profile 2 is shown in Fig. 6 and Table IV. Once again, the quality of the fit is good and, as above, the slight overestimate in intensity in the region of $8.5<s<9.5\ \mathrm{nm}^{-1}$ results in an artificial component of large icosahedra in the fitted size distribution. Had it been possible to use, in the calculation of basis functions, relaxed structures, we would expect this artifact to disappear.

The corresponding size distributions, shown in Fig. 7, indicate a predominance of icosahedra. For comparison, a sample of particles was also taken from the beam and the size distributions measured by TEM. The distribution obtained by microscopy is shown in Fig. 8. The maximum

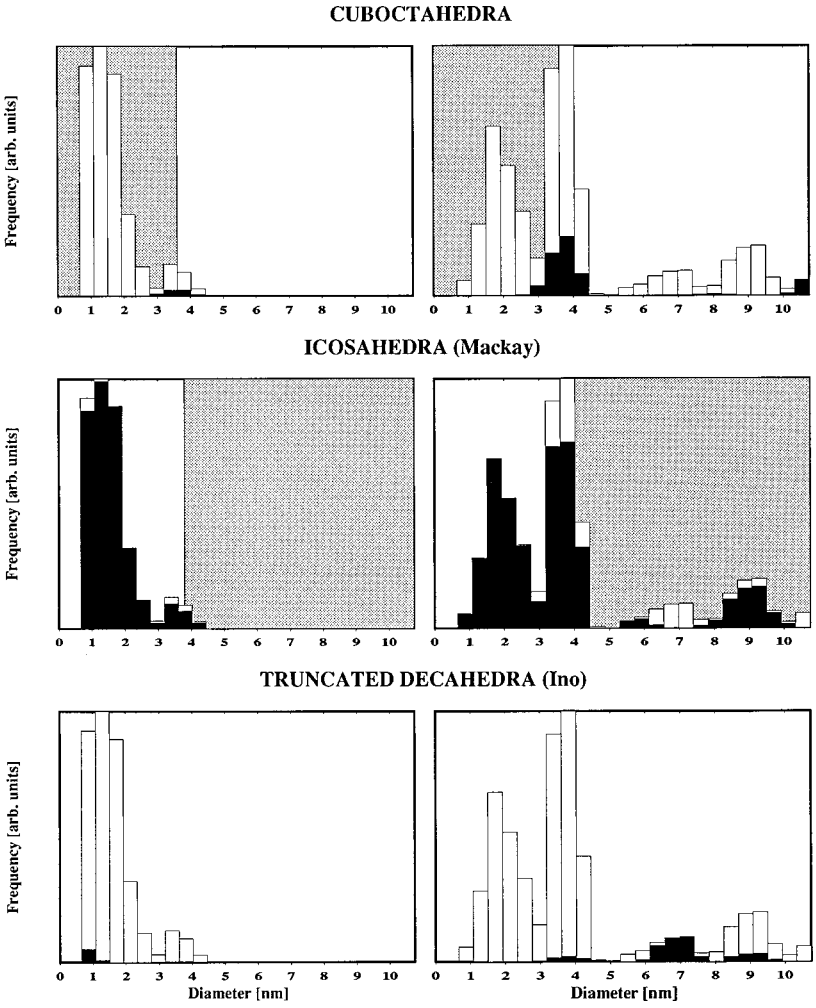

FIG. 7. Size distribution information about model structures used in the particular fit to profile 2 presented in Fig. 6 and Table IV. The presentation of data is described in the caption to Fig. 5.

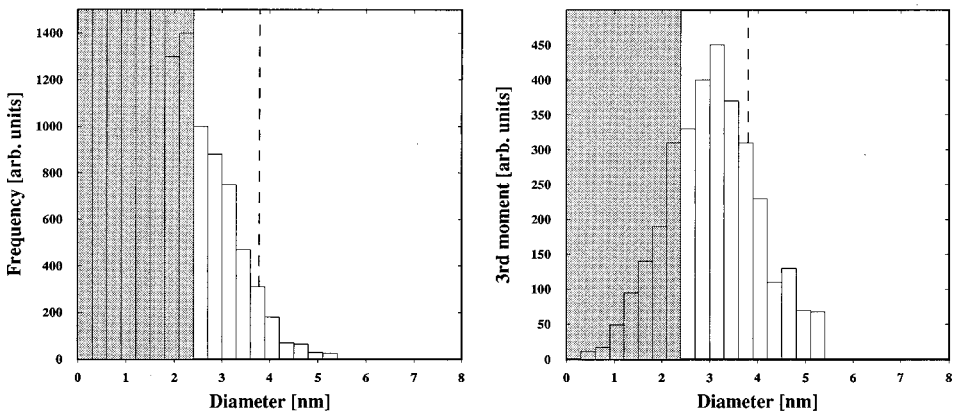

FIG. 8. Size distribution information obtained by electron microscopy on a supported sample taken during the acquisition of profile 2 (see Fig. 6). On the left: frequency histogram of particle sizes. On the right: histogram of volume-weighted frequencies (relative contributions to the total diffracted intensity). The gray regions indicate the size range in which the contrast arising from particles cannot be distinguished from the amorphous-carbon substrate. The dashed line locates the predicted icosahedra ⇔ fcc crossover size (Ref. 9).

particle diameter determined by microscopy is ≈5.5 nm. The mean diameter by fitting is 2.0 nm, and the third moment 3.8 nm, compared to 3.1 nm and 3.5 nm, respectively, by microscopy. The artificially high third moment in the fitted data is due to the inclusion of large icosahedra in the fit. These, as stated, are artifacts associated with the relaxation of the icosahedral structures: eliminating them from the third moment calculation results in a value below that obtained by microscopy.

In any comparison between fitted size distributions and distributions obtained by TEM, we would expect a systematic underestimation in the sizes obtained by fitting. This is due to the fact that the diffraction pattern recorded is only characteristic of the size and structure of coherent domains within a small particle. In general, the imperfect structure of many clusters will mean that they appear smaller in the analysis based on diffraction data. The external size and shape of a small particle contribute directly to small-angle scattering in a diffraction experiment, which is not accessible to us.

C. Cluster temperature

The average carrier gas temperature in the source chamber has been measured to be 500±50 K. This value is reasonably insensitive to changes in crucible temperature, making it a fair estimate of temperature in all the experimental data presented here. It has been used to calculate the Debye-Waller factor for the model profiles used in fitting (see Appendix B). The agreement obtained in using these functions to fit the experimental data is further reason to be confident that this temperature is reasonable.

In the diffraction profile 5 of Fig. 1, there is a perceptible horizontal shift of the experimental data with respect to the calculated profile. This indicates that the particles' lattice parameter differs from the bulk, room-temperature, value used to generate the calculated profile. Careful rescaling of the pattern shows the lattice to be dilated by 0.3±0.1% with respect to bulk copper at room temperature. According to bulk parameters,[22] a lattice expansion of 0.364% is expected at a temperature of 500 K: a full MD simulation of a copper crystal at 500 K shows a lattice expansion of 0.385%. Agreement here indicates that our estimate of cluster temperature is justified *a posteriori*, and confirms that clusters are thermalized with the buffer gas in the source chamber. Furthermore, our data suggest that there is no contraction in the lattice parameter caused by the small size of the clusters (diameter of 4.0±0.5 nm). This contradicts some previously reported results[23,24] but agrees with others[25,26]: it is supported by MD simulation in this study.

IV. DISCUSSION

An important feature of these experiments is that the conditions of particle growth were much slower than in previous studies.[17] We believe that particles grew relatively slowly while drifting through an extended vapor-rich region within the source chamber. There is evidence for this in the observed correlation between particle residence time in the source and mean particle size (see Appendix C). In our previous work, such behavior has not been observed and we estimate that growth rates here are at least an order of magnitude less than in earlier studies. In view of this, it is reasonable to expect that the particle structures observed reflect tendencies in thermodynamic stability, rather than kinetic factors. Indeed, the fact that a size-related structural effect is observed, and that it agrees with theoretical predictions, supports this hypothesis.

The evolution of diffraction features in the series of profiles shown in Fig. 1 are associated with a general trend in mean particle size: small in the front (profile 1) to large at the back (profile 5), which is correlated with carrier gas through-

TABLE IV. Size-distribution statistics for the fit to profile 2 represented in Figs. 6 and 7. The meaning of statistical parameters is described in the caption to Table III.

	$\overline{D}^{(i)}$ (nm)	$\overline{D}_V^{(i)}$ (nm)	$\eta^{(i)}$ (%)	$\gamma^{(i)}$ (%)
fcc	3.4	4.3	4	11
Icosahdera	1.9	3.4	96	81
Decahedra	4.9	6.6	1	8
total (white bars)	2.0	3.8		

put Q_g in the source. The same series is also associated with a change in the structural composition of the beam: icosahedra at the front (profile 1), through a mixture of MTP structures, to fcc cuboctahedra at the back (profile 5), by the detailed fitting analysis performed on the raw data. One might expect to see some correlation between the mean size of each structural component and Q_g. Indeed this is the case, we find in profiles 4 and 5, where an fcc component is significant, that the averaged mean size of fcc domains is significantly larger (4.2 nm) in profile 5 than in profile 4 (3.4 nm). We also find that in profiles 1, 2, and 3, where the MTP component is important, the averaged mean icosahedral domain size remains fairly constant (2.2 ± 0.3 nm). We would expect this to be the case because of the size limit on icosahedra, and the fact that we have not been able to produce particle beams in which the overall size distribution falls well below this size limit.

The presentation of our results in Fig. 3 shows most clearly the structural size effect in the experimental observations: on average the mean diameter of the icosahedral component is systematically smaller than the mean diameter of cuboctahedra. Furthermore, in Fig. 2, the icosahedral components are invariably within the size range of stability predicted by molecular-dynamics simulations.[9] However, in Fig. 2, the size of fcc particles is seen to fall partly below the line of critical stability. In considering this, it should be remembered that differences in the total energy of icosahedra and cuboctahedra are very small near the critical size and, therefore, the critical diameter determined on the basis of MD calculations cannot be taken too literally.[9] Several factors can, however, also explain the observed discrepancy.

Firstly, the finite temperature of particles under observation will tend to lower the critical size for the transition. This has been suggested in studies mapping out a phase diagram for small metal particle structures on the basis of HREM observations of gold particles.[27,28] The second concern is that, as we have already noted, there is a systematic difference between observed particle size and fitted domain sizes, the former being rather larger than the latter. This difference can be attributed to imperfect structure in particles, leading to diffraction from domains of smaller size than the host particle. It follows that the actual sizes of particles will, in general, be larger than those reported in Fig. 2 and Fig. 3.

It was recently proposed by van de Waal[29] that in the case of rare-gas clusters no size-dependent structural transition takes place as clusters grow in size. In support of this, a model structure has been developed that consists of a core atomic arrangement, with five-fold symmetry, on which further growth is compatible with fcc structures. At intermediate sizes, this model matches experimental diffraction profiles from argon clusters that could not previously be explained. We have not been able to test similar models against our own data in this study. However, several comments can be made. Firstly, we do obtain very satisfactory fits to our experimental data using the three basic structure types. These structures are known, from extensive HREM work, to exist in abundance in similar fcc metals. In the case of rare-gas cluster studies, van de Waal acknowledges that no satisfactory fit could be obtained in this way, thereby strengthening the case for his model in that system. Secondly, van de Waal's model gives rise to a decahedral core, not an icosahedral one. The problem that we already have in unambiguously identifying the decahedral component in our beam would make it difficult, if not impossible, to identify the van de Waal structure if it were present (it must be remembered that size distributions in rare-gas experiments are much narrower than with the IGA source).

Given that a structural transformation occurs, the question arises as to how such a transformation proceeds: if icosahedra exist plentifully only at small sizes then they must somehow rearrange their structure with increasing size. The results of this study do not give any direct insights into the mechanism involved. However, the original MD study that identified the critical size for the structural transition[9] did also note that a small complete-shelled fcc cluster (309 atoms) transformed, nondiffusively, into an icosahedron at all temperatures up to its melting temperature (900 K). On the other hand, a fcc cluster with an incomplete outer shell (219 atoms) failed to undergo a transition, in the time scale of the simulation, right up to its melting point. Such results indicate that as particles grow there may well be opportunities for structural transition with little or no activation energy barrier. Furthermore, there is considerable experimental evidence, from electron microscopy studies, that particles are able to undergo structural changes between the three competing structure types.[30,27,28] In these observations, considerable energy must be supplied to initiate a ''quasimolten'' state in which rapid changes in structure occur. Thereafter, however, very little external stimulus is needed to maintain the activity and it has been suggested that the initial energy is required only to overcome interactions with the substrate.[27] Again, although the energy barriers for the different structural transitions are not known, it has been argued that these fluctuations will occur at temperatures significantly below particle melting temperatures.[28] In so doing, individual particles ''sample'' their configuration space and are more likely to be observed in the lowest-energy structure.

The observation of a size-related structure transition in copper contradicts an earlier study involving copper clusters supported in a matrix of solid argon.[26] In that study, EXAFS was used to probe cluster structure and Fourier inversion used to obtain the sample pair-distribution functions, which were then compared with theoretical coordination numbers obtained from simple structure models. Since the publication of those findings, however, there has been some discussion in the literature regarding the interpretation of EXAFS in small particles[11] and also the identification of structure, after Fourier inversion, from details in the pair distribution function.[8] In comparing the present to the EXAFS study, both used the inert-gas-aggregation method to generate clusters, although the present study observed free clusters, whereas the EXAFS one required a matrix support. Both studies obtain information directly in reciprocal space, in the present study the analysis has also been carried out in reciprocal space (by calculating the appropriate diffraction patterns of model structures), whereas in the EXAFS study a delicate inversion procedure was applied to form a real-space representation of sample interatomic distances, which were then compared with single models of structure. We are not aware of other studies concerning copper clusters of comparable size to the present study. One recent study of gas ab-

sorption on rather smaller free copper clusters showed icosahedra in the size range between 70 and 95 atoms.[31]

A recurring question in structural studies of small metal particles is the occurrence, or not, of a size-dependent contraction in the crystal lattice parameter. We believe that the possible presence of a mixture of structures in samples makes interpretation of experimental measurements very tricky. Only one set of data in this study is suitable for some comment. In Sec. III C we have used an apparent thermal expansion of 0.3% in the fcc copper lattice to estimate the temperature of clusters in the particle beam. We used the data of profile 5, in Fig. 1, which are dominated by fcc clusters and for which the mean diameter by fitting is 4.0 ± 0.5 nm. There is agreement among MD simulation, our experimental data, and the expected expansion of bulk copper at 500 K. This suggests that if any size-related *lattice contraction* is present it must be considerably smaller than the thermal expansion in particles of this size. This is in agreement with the results of a study by Montano *et al.*,[26] although not so with the work of De Crescenzi *et al.*[24] and Apai *et al.*[23] who found lattice contractions of about 1% in supported copper clusters of similar size.

V. CONCLUSION

Electron diffraction has been used in this study to probe the structure of unsupported clusters of copper, grown in an inert-gas-aggregation source. The experimental conditions are well suited to the study of copper clusters because of the elimination of perturbations to the cluster's surface, such as substrate-contact and in particular oxidation. Furthermore, the conditions of particle growth were such that the observed tendency to form in different structures can be associated with the relative stability of such structures, rather than kinetic factors.

By detailed analysis of the experimental data, the composition of the particle beam in a particular measurement can be described in terms of the size distribution of structure types. These results have been compared with the predictions of an earlier MD study of copper clusters, predicting a size-dependent preference for icosahedra over fcc structures below a diameter of 3.8 nm.[9] A structural size effect is clearly observed. A distinct preference for icosahedral structure at small cluster sizes, and fcc structure at larger sizes, is seen in *all* measurements made. This is noteworthy, given that the range of source conditions was varied significantly. The observed critical size is in agreement with MD calculations, although slightly smaller than predicted.

In addition to the size effect, consistency between the experimental observations and simulations has been shown in two ways: Firstly, the dynamic behavior of cluster atoms, as simulated at finite temperature, and the Debye-Waller factor used in fitting to the experimental data are in good agreement. Secondly, a small lattice expansion observed in 4 nm fcc clusters was matched with a simulation of a similar cluster at the experimentally estimated temperature. These results also correlate well with independent estimates of carrier gas temperature in the IGA source.

The marriage of *in situ* electron diffraction measurements with detailed MD simulations provides a very effective tool with which to probe the structure of nanometer-sized metal particles. The results of MD calculations showing how large icosahedral structure relax has been very useful in this study, and in a recent study of silver clusters.[17] Molecular dynamics permits a more subtle interpretation of the detailed features of the diffraction patterns and fitting analyses than would otherwise be possible. It has also been possible to establish the validity of approximations used in analyzing raw experimental data, such as the use of the conventional Debye-Waller factor.

ACKNOWLEDGMENTS

The electron-microscopy contributions of D. Ugarte, obtained with the support of the Centre Interdépartemental de Microscopie Electronique at EPFL, are gratefully acknowledged. We would like to thank G. Torchet and M. Manninen for many valuable discussions. This work was supported by the Academy of Finland and the Swiss National Science Foundation.

APPENDIXES

The appendixes to this paper are rather extensive and concern only readers interested in some technical details. They are therefore being published separately, by the AIP's Physics Auxiliary Publication Service (PAPS), where they can be ordered.[18]

A brief summary of their contents follows.

APPENDIX A: FITTING CALCULATED DIFFRACTION PATTERNS TO EXPERIMENTAL DATA

This appendix describes specific aspects of the fitting procedure used in this study: calculation of diffraction profiles, the structure models used to calculate diffraction profiles, an explanation of the fitting procedure, the statistical parameters that are quoted as results, and a discussion of possible ambiguity in the results obtained by fitting.

APPENDIX B: MD SIMULATIONS AND DIFFRACTION

Appendix B presents the results of a molecular-dynamics (MD) study of the structure of copper clusters. It begins with an overview of the MD method, followed by general findings about the structure and dynamics of these clusters and a brief discussion on the stability of decahedral clusters. The consequences of the relaxation and dynamic behavior of real clusters in terms of the associated diffraction profiles are discussed.

APPENDIX C: RELATIONSHIP OF PARTICLE SIZE TO SOURCE CONDITIONS

This appendix addresses the relationship between particle size and source conditions, showing that the main parameter determining the mean size of particles produced in the experiments reported here is their time of residence in the evaporation chamber.

*Present address: Dépertement des matériaux, EPFL, 1015 Lausanne, Switzerland.
†Present address: Measurement Standards Laboratory, Industrial Research Ltd., Lower Hutt, New Zealand.
‡Present address: Observatoire Cantonal, 2000 Neuchâtel, Switzerland.
**Author to whom correspondence should be addressed.
§Present address: ABB Corporate Research Oy, P.O. Box 608, 65101 Vaasa, Finland.

[1] L. D. Marks, Rep. Prog. Phys. **57**, 603 (1994).
[2] P. Audit, J. Phys. (France) **30**, 192 (1969).
[3] A. Yokozeki and G. D. Stein, J. Appl. Phys. **49**, 2224 (1978).
[4] B. D. Hall, M. Flüeli, D. Reinhard, J. -P. Borel, and R. Monot, Rev. Sci. Instrum. **62**, 1481 (1991).
[5] B. Raoult, J. Farges, M. -F. de Feraudy, and G. Torchet, Philos. Mag. B **60**, 881 (1989).
[6] C. L. Cleveland and U. Landman, J. Chem. Phys. **94**, 7376 (1991).
[7] H. S. Lim, C. K. Ong, and F. Ercolessi, Surf. Sci. **269/270**, 1109 (1992).
[8] J. Uppenbrink and D. J. Wales, J. Chem. Phys. **96**, 8520 (1992).
[9] S. Valkealahti and M. Manninen, Phys. Rev. B **45**, 9459 (1992).
[10] C. L. Briant and J. J. Burton, J. Chem. Phys. **63**, 2045 (1975).
[11] L. B. Hansen, P. Stoltze, J. K. Nørskov, B. S. Clausen, and W. Niemann, Phys. Rev. Lett. **64**, 3155 (1990).
[12] F. Ercolessi, W. Andreoni, and E. Tosatti, Phys. Rev. Lett. **66**, 911 (1991).
[13] H. S. Lim, C. K. Ong, and F. Ercolessi, Z. Phys. D **26S**, 45 (1993).
[14] S. Valkealahti and M. Manninen, Comput. Mater. Sci. **1**, 123 (1993).
[15] J. Farges, M. -F. de Feraudy, B. Raoult, and G. Torchet, J. Chem. Phys. **84**, 3491 (1986).
[16] B. D. Hall, M. Flüeli, R. Monot, and J. -P. Borel, Phys. Rev. B **43**, 3906 (1991).
[17] D. Reinhard, B. D. Hall, D. Ugarte and R. Monot, Phys. Rev. B **55**, 7868 (1997).
[18] See Document No. PAPS PRBMD0-58-072828 for Appendixes. Order by PAPS number in the journal reference from American Institute of Physics, Physics Auxiliary Publication Service, 500 Sunnyside Boulevard, Woodbury, NY 11797-2999. Fax: 516-576-2223, e-mail: paps@aip.org. The price is $1.50 for each microfiche (98 pages) or $5.00 for photocopies of up to 30 pages, and $0.15 for each additional page over 30 pages. Airmail additional. Make checks payable to the American Institute of Physics.
[19] W. H. Press, S. A. Teukolsky, W. T. Vetterling, and B. P. Flannery, *Numerical Recipes in C: The Art of Scientific Computing* (Cambridge, Cambridge UK, 1992).
[20] Particle diameter D as a function of the number of atoms: $D(561)=2.3$ nm; $D(1289)=3.1$ nm; $D(2057)=3.6$ nm; $D(3000)=4.1$ nm; $D(8217)=5.7$ nm; $D(10000)=6.1$ nm.
[21] B. D. Hall, Thesis No. 954, Ecole Polytechnique Fédérale de Lausanne (1991) (unpublished).
[22] D. E. Gray, *The American Institute of Physics Handbook* (McGraw-Hill, New York, 1972).
[23] G. Apai, J. F. Hamilton, J. F. Stohr, and A. Thompson, Phys. Rev. Lett. **43**, 165 (1979).
[24] M. De Crescenzi, M. Diociaiuti, L. Lozzi, P. Picozzi, and S. Santucci, Phys. Rev. B **35**, 5997 (1987).
[25] H. J. Wasserman and J. S. Vermaak, Surf. Sci. **32**, 168 (1972).
[26] P. A. Montano, G. K. Shenoy, E. E. Alp, W. Schulze, and J. Urban, Phys. Rev. Lett. **56**, 2076 (1986).
[27] P. M. Ajayan and L. D. Marks, Phys. Rev. Lett. **60**, 585 (1988).
[28] N. Doraiswamy and L. D. Marks, Philos. Mag. B **71**, 291 (1995).
[29] B. W. van de Waal, Phys. Rev. Lett. **76**, 1083 (1996).
[30] S. Iijima and T. Ichihashi, Phys. Rev. Lett. **56**, 616 (1986).
[31] E. K. Parks, L. Zhu, J. Ho, and S. J. Riley, Z. Phys. D **26**, 41 (1993).
[32] A. Roth, *Vacuum Technology* (North-Holland, Amsterdam, 1982).